Bifunctional Water-Splitting Electrocatalysis Achieved by Defect-Order in $LaA_2Fe_3O_8$ (A = Ca, Sr)

Surendra B. Karki[a], Antonis N. Andriotis[b], Madhu Menon[c,d], Farshid Ramezanipour[a,*]

[a]Department of Chemistry, University of Louisville, Louisville, Kentucky 40292, USA
[b]Institute of Electronic Structure and Laser, FORTH, Heraklio, Crete, Greece
[c]Conn Center for Renewable Energy Research, University of Louisville, Louisville, KY 40292, USA
[d]Department of Physics and Astronomy, University of Kentucky, Lexington, KY 40506, USA

Supporting Information Placeholder

ABSTRACT: We report the utilization of defect-order for development of a bifunctional oxide electrocatalyst. This structure-activity relationship is demonstrated through a disorder-order transformation in $LaA_2Fe_3O_8$ (A = Ca, Sr). The defect-ordered oxide, $LaCa_2Fe_3O_8$, shows electrocatalytic activity for oxygen-evolution reaction, on par with that of the state-of-the-art precious metal catalyst RuO_2. In addition, it is capable of catalyzing the other half reaction of water-splitting, namely hydrogen evolution reaction. Importantly, it is an iron-based catalyst and can be used as a single phase bulk material. The most important aspect of this work is the pronounced impact of defect-order on electrocatalytic properties of oxides.

Keywords: Electrocatalysis, Water-splitting, Bifunctional, Structural Order, OER, HER

Electrochemical water splitting technology is hindered by the sluggish kinetics of the two half reactions of this process, namely hydrogen evolution reaction (HER) and oxygen evolution reaction (OER). Precious metal catalysts, such as Pt and RuO_2, are often utilized to enhance these reactions. The high cost of such catalysts has motivated the search for sustainable alternatives based on earth-abundant elements. Oxide materials, especially perovskite-type oxides, can be excellent candidates for application as electrocatalysts due to their stability and high degree of tunability. Several materials from this family have shown significant OER activity.[1-3] The HER activity of perovskite oxides is less common, but some materials from this family have been studied for HER catalysis.[3-5] However, perovskite oxides that can catalyze both OER and HER are rare, especially in bulk form without nanofabrication or composite formation.[6]

Following our recent work on oxide electrocatalysts,[2-4, 7-9] we now demonstrate the realization of these properties in perovskite oxides through creation of structural order in materials with formulae $LaSr_2Fe_3O_8$ (disordered) and $LaCa_2Fe_3O_8$ (ordered). These compounds are derived from the oxygen-deficient perovskite $ABO_{3-\delta}$, where $\delta = 1/3$. Therefore, the general formula can be represented as $La_{1/3}A_{2/3}FeO_{3-1/3}$ or $LaA_2Fe_3O_8$ (A=Ca,Sr). In the disordered compound, $LaSr_2Fe_3O_8$, the distribution of oxygen-vacancies is random and the average structure resembles that of a typical perovskite (Figure 1a), but with partial occupancy on oxygen sites (Table S1). On the other hand, $LaCa_2Fe_3O_8$ has a structure where the oxygen-vacancies are distributed in an ordered fashion. Indeed, the level of oxygen-deficiency found in these compounds, i.e., $\delta = 1/3$, has the potential to create an ordered arrangement if the oxygen-vacancies only appear in every third layer of the perovskite structure, converting the octahedral coordination into tetrahedral (Figure 1b). Such arrangement also results in two different coordination numbers for the A-sites, CN = 8 and CN = 12. We postulated that this type of ordering may be achieved through incorporation of a smaller A-site cation, Ca^{2+}, which can comfortably reside in the 8-coordinated site, leaving the 12-coordnated site to La^{3+}. Note that the stoichiometric ratio of CN = 12 to CN = 8 sites is 1:2, hence the composition $LaCa_2Fe_3O_8$, which can accommodate the targeted ordering scheme. Figure S1 and Table S2 show the Rietveld refinement results, consistent with an earlier structural report.[10] Iodometric titrations were also used to confirm the oxygen stoichiometry.

The transformation of the crystal structure from disordered to ordered results in remarkable changes to electrocatalytic properties. There is a significant enhancement of the HER activity from $LaSr_2Fe_3O_8$ (disordered) to $LaCa_2Fe_3O_8$ (ordered), as shown in Figure 2. The latter compound shows overpotential of $\eta_{10} = 0.4$ V in 1 M KOH. This is close to the values reported for some other oxygen-deficient perovskites, such as $Ba_{0.5}Sr_{0.5}Co_{0.8}Fe_{0.2}O_{3-\delta}$[11] and $Ba_{0.95}Co_{0.4}Fe_{0.4}Zr_{0.1}Y_{0.1}O_{3-\delta}$.[11] It is also significant that $LaCa_2Fe_3O_8$ is able to catalyze the HER in bulk form, without any need for composite formation or nanofabrication. Even more sig-

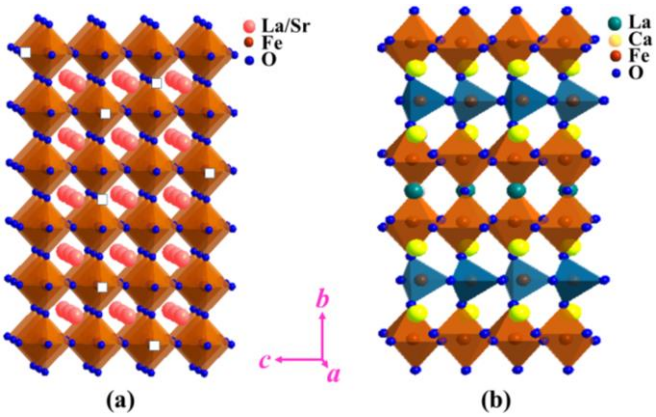

Figure 1: (a) Perovskite structure with random vacancy distribution for $LaSr_2Fe_3O_8$. White squares are a schematic representation of the random distribution of oxygen-vacancies. (b) Ordered structure of $LaCa_2Fe_3O_8$, with vacancies only appearing in every third layer, hence creating FeO_4 tetrahedral coordination in every third layer.

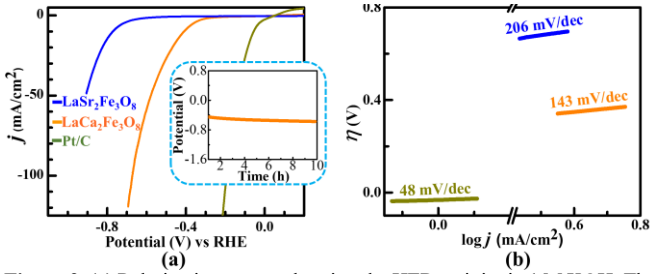

Figure 2. (a) Polarization curves showing the HER activity in 1 M KOH. The inset shows the chronopotentiometry data for $LaCa_2Fe_3O_8$. (b) Tafel plots and Tafel slopes.

nificant is the structure-property relationship, where the electrocatalytic activity is enhanced as a function of structural transformation from disorder to order. We note that this catalyst also shows better HER activity than the non-defect oxide $LaFeO_3$, as shown in Figure S3. $LaCa_2Fe_3O_8$ is also very stable, as demonstrated by chronopotentiometry data presented in the inset of Figure 2a. The Tafel slope, i.e., the slope of η versus log j, based on the Tafel equation, $\eta = a + b \log j$, is commonly used to evaluate the HER kinetics.[12, 13] Smaller Tafel slopes indicate faster reactions. The Tafel plots in Figure 2b show that the reaction kinetics are also enhanced as a function of structural order, with $LaCa_2Fe_3O_8$ showing a smaller Tafel slope.

Remarkably, these catalysts also show electrocatalytic activity for the other half-reaction of water-splitting, namely OER (Figure 3). The structure-property relationships are on full display, where the transition from disorder to order leads to a significant enhancement in OER activity from $LaSr_2Fe_3O_8$ (disordered) to $LaCa_2Fe_3O_8$ (ordered). The latter material shows an outstanding activity for OER, on par with the state-of-the-art precious metal electrocatalyst, RuO_2. It shows an overpotential of $\eta_{10} = 0.36$ V in 1M KOH, on par with that of RuO_2 (Figure 3a).[14-16] It is also highly stable, as shown by chronopotentiometry experiments presented in the inset of Figure 3a. In addition, X-ray diffraction and X-ray photoelectron spectroscopy before and after electrocatalytic reaction (Figures S4 and S5) indicate the structural stability of this catalyst. The kinetics of the OER was evaluated using the Tafel plot,[17, 18] indicating the enhancement of kinetics, where $LaCa_2Fe_3O_8$ shows a smaller Tafel slope, consistent with faster charge transport during OER.[2, 19]

The electrochemically active surface areas (ECSA) were also evaluated by examining the electrochemical double-layer capacitance (C_{dl}) in the non-faradaic region of the voltammograms (Figure S6).[6, 20] In this region, the electrode reactions are considered negligible and the current originates from electrical double layer charge and discharge.[20] ECSA and C_{dl} are related to each other by ECSA = C_{dl} / C_s ,[2, 21] where C_s is the specific capacitance. Given this direct relationship, the C_{dl} is typically considered to be representative of the magnitude of ECSA.[2, 22] The value of C_{dl} is calculated from the equation[23, 24] $C_{dl} = \Delta j / \nu$, where Δj is the absolute value of the difference between the anodic (j_{anodic}) and cathodic ($j_{cathodic}$) current densities from the flat regions of the CV in the non-faradic region and ν is the scan rate. The C_{dl} value is equivalent to half of the slope of Δj versus ν plot.[22, 24] Alternatively, some reports have used $j_{average}$ versus ν, where $j_{average}$ is the average of the absolute values of j_{anodic} and $j_{cathodic}$. In that case, C_{dl} is simply equal to the slope of the $j_{average}$ versus ν plot.[25, 26] Figure 3c shows the C_{dl} values obtained using $j_{average}$ at middle potential[13] of the non-Faradaic CVs. The C_{dl} value for $LaCa_2Fe_3O_8$ is similar to that of RuO_2, and significantly larger than that of $LaSr_2Fe_3O_8$, consistent with high electrocatalytic activity of $LaCa_2Fe_3O_8$.

The novel and intriguing nature of the observed trends in electrocatalytic activity as a function of structural order prompted us to employ density-functional-theory (DFT) to examine the changes in electronic structure due to the ordering (Figure 4). The electronic band structure for $LaSr_2Fe_3O_8$ indicates the crossing of a few spin-up bands through the Fermi level, implying a half-metallic character. On the other hand, the band structure for $LaCa_2Fe_3O_8$ shows a semiconducting behavior with a small band gap and no bands crossing the Fermi level.

Several OER descriptors, such as proximity of the transition metal d and oxygen p band centers[27] and hybridization between them, [27, 28] have been proposed. The degree of hybridization between Fe d and O p bands is indicated by the overlap area of the DOS of these bands,[28] normalized based on all participating orbitals in the supercell. For $LaSr_2Fe_3O_8$, the Fe d and O p overlap areas are 0.666 (spin up) and 0.288 (spin down). The corresponding values for $LaCa_2Fe_3O_8$ are 0.562 (spin up) and 0.295 (spin down). Some researchers have focused on the proximity of the d-band center to the Fermi level and have correlated this parameter with enhanced electrocatalytic activity due to enhanced bonding with adsorbates.[29, 30] The DOS shows that the average d-band center (for both spin up and down) is -5.285 eV for $LaSr_2Fe_3O_8$ and -5.191 eV for $LaCa_2Fe_3O_8$. These differences are a result of the structural differences between the two systems. The coordination number of metal atoms and the directions of the bonds will be different between the disordered and ordered systems. Similar effects on catalytic activity have been previously observed in other contexts, such as CO oxidation.[31] Furthermore, it is evident from the partial density of states (PDOS) in Figure 4 that unlike O p-bands that are similar in both disordered $LaSr_2Fe_3O_8$ and ordered $LaCa_2Fe_3O_8$, there is a difference in the localization of Fe d-bands, which are more localized in $LaCa_2Fe_3O_8$.

In summary, this work demonstrates the rational design of a highly active electrocatalyst for water-splitting by creation of structural order. The transition from disorder to order leads to the transformation of the electrocatalytic properties, where the activity of the ordered system rivals that of the state-of-the-art precious metal electrocatalysts. We expect this structure-property principle

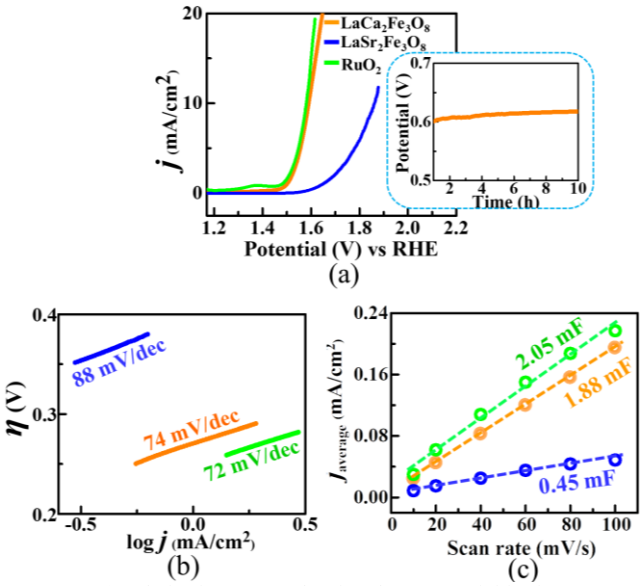

Figure 3. (a) Polarization curves showing the OER activities in 1M KOH. Inset shows chronopotentiometry for $LaCa_2Fe_3O_8$. (b) Tafel plots. (c) Double layer capacitance values, C_{dl}, obtained from CVs in non-Faradaic region.

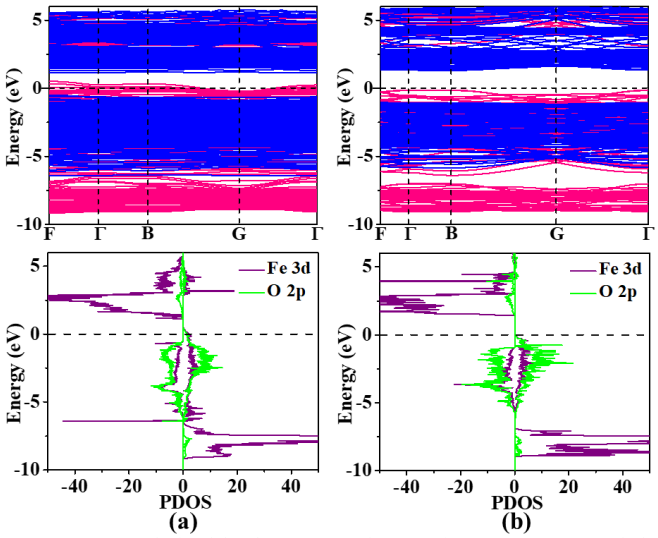

Figure 4. DFT calculated band structure and PDOS for (a) $LaSr_2Fe_3O_8$ and (b) $LaCa_2Fe_3O_8$. The energy of the Fermi-level is set to zero. In band structures, red and blue lines denote contributions from spin-up and spin-down electrons, respectively.

to be applicable to a wide range of oxide materials given that structural order also affects the electronic structure. Currently, we are exploring several other series of oxygen-deficient perovskites to show the relationship between structural order and electrocatalytic activity.

ASSOCIATED CONTENT

Supporting Information

The Supporting Information is available free of charge on the ACS Publications website.

Experimental procedures; DFT methods; Rietveld refinement profiles; HER and OER data under different conditions; X-ray diffraction data before and after OER; CVs for obtaining C_{dl}, DFT charge plots (PDF)

AUTHOR INFORMATION

Corresponding Author

Farshid Ramezanipour- Department of Chemistry, University of Louisville, Louisville, Kentucky 40292, Unite States, ORCID iD: 0000-0003-4176-1386. Email: farshid.ramezanipour@louisville.edu

ACKNOWLEDGMENT

This work is supported in part by the National Science Foundation (NSF) under grant no. DMR-1943085.

REFERENCES

1. Suntivich, J.; May, K. J.; Gasteiger, H. A.; Goodenough, J. B.; Shao-Horn, Y., A Perovskite Oxide Optimized for Oxygen Evolution Catalysis from Molecular Orbital Principles. *Science* **2011,** *334*, 1383.

2. Hona, R. K.; Ramezanipour, F., Remarkable Oxygen-Evolution Activity of a Perovskite Oxide from the $Ca_{2-x}Sr_xFe_2O_{6-\delta}$ Series. *Angew. Chem.* **2019,** *58*, 2060-2063.

3. Hona, R. K.; Karki, S. B.; Ramezanipour, F., Oxide Electrocatalysts Based on Earth-Abundant Metals for Both Hydrogen- and Oxygen-Evolution Reactions. *ACS Sustainable Chem. Eng.* **2020,** *8*, 11549-11557.

4. Karki, S. B.; Ramezanipour, F., Pseudocapacitive Energy Storage and Electrocatalytic Hydrogen-Evolution Activity of Defect-Ordered Perovskites $Sr_xCa_{3-x}GaMn_2O_8$ (x = 0 and 1). *ACS Appl. Energy Mater.* **2020,** *3*, 10983-10992.

5. Xu, X.; Chen, Y.; Zhou, W.; Zhu, Z.; Su, C.; Liu, M.; Shao, Z., A Perovskite Electrocatalyst for Efficient Hydrogen Evolution Reaction. *Adv. Mater.* **2016,** *28*, 6442-6448.

6. Wang, J.; Gao, Y.; Chen, D.; Liu, J.; Zhang, Z.; Shao, Z.; Ciucci, F., Water Splitting with an Enhanced Bifunctional Double Perovskite. *ACS Catal.* **2018,** *8*, 364-371.

7. Hona, R. K.; Ramezanipour, F., Structure-dependence of electrical conductivity and electrocatalytic properties of $Sr_2Mn_2O_6$ and $CaSrMn_2O_6$. *J. Chem. Sci.* **2019,** *131* (11), 109.

8. Hona, R. K.; Ramezanipour, F., Effect of the Oxygen Vacancies and Structural Order on the Oxygen Evolution Activity: A Case Study of $SrMnO_{3-\delta}$ Featuring Four Different Structure Types. *Inorg. Chem.* **2020,** *59*, 4685-4692.

9. Alom, M. S.; Ramezanipour, F., Layered Oxides $SrLaFe_{1-x}Co_xO_{4-\delta}$ (x=0–1) as Bifunctional Electrocatalysts for Water-Splitting. *ChemCatChem* **2021,** *13*, 3510-3516.

10. Guo, H.; Hosaka, Y.; Romero, F. D.; Saito, T.; Ichikawa, N.; Shimakawa, Y., Two Charge Ordering Patterns in the Topochemically Synthesized Layer-Structured Perovskite $LaCa_2Fe_3O_9$ with Unusually High Valence $Fe^{3.67+}$. *Inorg. Chem.* **2017,** *56*, 3695–3701.

11. Li, X.; He, L.; Zhong, X.; Zhang, J.; Luo, S.; Yi, W.; Zhang, L.; Hu, M.; Tang, J.; Zhou, X.; Zhao, X.; Xu, B., Evaluation of A-Site Ba^{2+}-Deficient $Ba_{1-x}Co_{0.4}Fe_{0.4}Zr_{0.1}Y_{0.1}O_{3-\delta}$ Oxides as Electrocatalysts for Efficient Hydrogen Evolution Reaction. *Scanning* **2018,** *2018*, 1341608-1341608.

12. Bard, A. J.; Faulkner, L. R., *Electrochemical Methods: Fundamentals and Applications*; Wiley, 2000.

13. Oh, S.; Kim, H.; Kwon, Y.; Kim, M.; Cho, E.; Kwon, H., Porous Co–P foam as an efficient bifunctional electrocatalyst for hydrogen and oxygen evolution reactions. *J. Mater. Chem. A* **2016,** *4*, 18272-18277.

14. Tahir, M.; Pan, L.; Zhang, R.; Wang, Y.-C.; Shen, G.; Aslam, I.; Qadeer, M. A.; Mahmood, N.; Xu, W.; Wang, L.; Zhang, X.; Zou, J.-J., High-Valence-State NiO/Co_3O_4 Nanoparticles on Nitrogen-Doped Carbon for Oxygen Evolution at Low Overpotential. *ACS Energy Lett.* **2017,** *2*, 2177-2182.

15. Fan, Z.; Liao, F.; Shi, H.; Liu, Y.; Shao, M.; Kang, Z., Highly efficient water splitting over a RuO_2/F-doped graphene electrocatalyst with ultra-low ruthenium content. *Inorg. Chem. Front.* **2020,** *7*, 2188-2194.

16. Das, D.; Nanda, K. K., One-step, integrated fabrication of Co_2P nanoparticles encapsulated N, P dual-doped CNTs for highly advanced total water splitting. *Nano Energy* **2016,** *30*, 303-311.

17. Lee, Y.; Suntivich, J.; May, K. J.; Perry, E. E.; Shao-Horn, Y., Synthesis and Activities of Rutile IrO_2 and RuO_2 Nanoparticles for Oxygen Evolution in Acid and Alkaline Solutions. *J. Phys. Chem. Lett* **2012,** *3*, 399-404.

18. Zhu, Y.; Zhou, W.; Chen, Z.-G.; Chen, Y.; Su, C.; Tadé, M. O.; Shao, Z., $SrNb_{0.1}Co_{0.7}Fe_{0.2}O_{3-\delta}$ Perovskite as a Next-Generation Electrocatalyst for Oxygen Evolution in Alkaline Solution. *Angew. Chem* **2015,** *54*, 3897-3901.

19. Song, F.; Hu, X., Ultrathin Cobalt–Manganese Layered Double Hydroxide Is an Efficient Oxygen Evolution Catalyst. *J. Am. Chem. Soc.* **2014,** *136*, 16481-16484.

20. Li, L.; Qin, Z.; Ries, L.; Hong, S.; Michel, T.; Yang, J.; Salameh, C.; Bechelany, M.; Miele, P.; Kaplan, D.; Chhowalla, M.; Voiry, D., Role of Sulfur Vacancies and Undercoordinated Mo Regions in MoS_2 Nanosheets toward the Evolution of Hydrogen. *ACS Nano* **2019,** *13*, 6824-6834.

21. Shinagawa, T.; Garcia-Esparza, A. T.; Takanabe, K., Insight on Tafel slopes from a microkinetic analysis of aqueous electrocatalysis for energy conversion. *Sci. Rep.* **2015,** *5*, 13801-13801.

22. Pan, Y.; Chen, Y.; Li, X.; Liu, Y.; Liu, C., Nanostructured nickel sulfides: phase evolution, characterization and electrocatalytic properties for the hydrogen evolution reaction. *RSC Adv.* **2015,** *5*, 104740-104749.

23. McCrory, C. C. L.; Jung, S.; Peters, J. C.; Jaramillo, T. F., Benchmarking Heterogeneous Electrocatalysts for the Oxygen Evolution Reaction. *J. Am. Chem. Soc.* **2013,** *135*, 16977-16987.

24. Zhang, B.; Lui, Y. H.; Zhou, L.; Tang, X.; Hu, S., An alkaline electro-activated Fe–Ni phosphide nanoparticle-stack array for high-performance oxygen evolution under alkaline and neutral conditions. *J. Mater. Chem. A* **2017,** *5*, 13329-13335.

25. Zhu, Y.; Zhou, W.; Sunarso, J.; Zhong, Y.; Shao, Z., Phosphorus-Doped Perovskite Oxide as Highly Efficient Water Oxidation

Electrocatalyst in Alkaline Solution. *Adv. Funct. Mater* **2016,** *26*, 5862-5872.
26. Petrie, J. R.; Cooper, V. R.; Freeland, J. W.; Meyer, T. L.; Zhang, Z.; Lutterman, D. A.; Lee, H. N., Enhanced Bifunctional Oxygen Catalysis in Strained $LaNiO_3$ Perovskites. *J. Am. Chem. Soc.* **2016,** *138*, 2488-2491.
27. Song, J.; Wei, C.; Huang, Z.-F.; Liu, C.; Zeng, L.; Wang, X.; Xu, Z. J., A review on fundamentals for designing oxygen evolution electrocatalysts. *Chem. Soc. Rev.* **2020,** *49*, 2196-2214.
28. Li, H.; Sun, S.; Xi, S.; Chen, Y.; Wang, T.; Du, Y.; Sherburne, M.; Ager, J. W.; Fisher, A. C.; Xu, Z. J., Metal–Oxygen Hybridization Determined Activity in Spinel-Based Oxygen Evolution Catalysts: A Case Study of $ZnFe_{2-x}Cr_xO_4$. *Chem. Mater.* **2018,** *30*, 6839-6848.
29. Sun, Y.; Zhao, Z.; Wu, S.; Li, W.; Wu, B.; Liu, G.; Chen, G.; Xu, B.; Kang, B.; Li, Y.; Li, C., Engineering of the d-Band Center of Perovskite Cobaltite for Enhanced Electrocatalytic Oxygen Evolution. *ChemSusChem* **2020,** *13*, 2671-2676.
30. Sun, S.; Zhou, X.; Cong, B.; Hong, W.; Chen, G., Tailoring the d-Band Centers Endows $(Ni_xFe_{1-x})_2P$ Nanosheets with Efficient Oxygen Evolution Catalysis. *ACS Catal.* **2020,** *10*, 9086-9097.
31. Mpourmpakis, G.; Andriotis, A. N.; Vlachos, D. G., Identification of Descriptors for the CO Interaction with Metal Nanoparticles. *Nano Lett.* **2010,** *10*, 1041-1045.

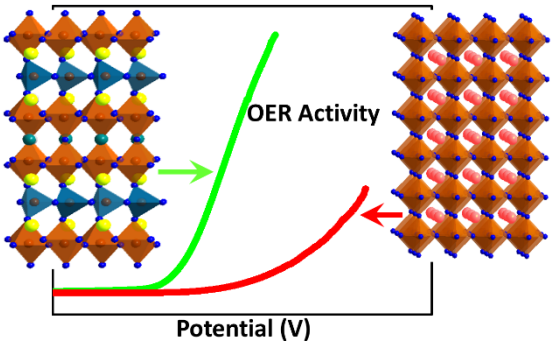
OER Activity
Potential (V)